**Atmospheric
Chemistry
and Physics**

Relationships between mineral dust and cloud properties in the West African Sahel

L. Klüser[1,2] **and T. Holzer-Popp**[1]

[1]German Aerospace Center (DLR), German Remote Sensing Datacenter (DFD), Wessling, Germany
[2]University of Augsburg, Institute of Physics, Augsburg, Germany

Abstract. Aerosol cloud interactions are known to be of great importance to many parts of the climate system. Five years of observations from three different satellites (Aqua, ENVISAT and Meteosat Second Generation) are used to statistically analyse the relationship of mineral dust aerosol, separated from other aerosol species, with monsoon season cloud state in the West African Sahel domain. Additionally, observations of the Tropical Rainfall Measuring Mission are used for discrimination of dry and wet seasons. The aerosol-cloud-interactions are analysed separately by season and air mass in order to minimise spurious correlations with meteorological conditions. The detailed analysis uncovers different counteracting relationships of the mineral dust aerosol with the cloud state, which is also evident from an analysis of the spatial distribution patterns of cloud properties changes with dust activity. The aerosol-cloud relationships found from the analysis of this multiple year dataset are mainly consistent with the hypothesis of a suppression of convective activity, but also indications of lifetime enhancement and thus increased cloud cover and convective intensity are found in some subsets.

1 Introduction

Atmospheric aerosols have strong influence on in-cloud processes and thus on resulting cloud properties (Twomey, 1974; Kaufman and Fraser, 1997; Ramanathan et al., 2001; Rosenfeld, 2006; Klüser et al., 2008; Stevens and Feingold, 2009). In the West African Sahel domain, cloud state and rainfall are mainly dominated by the West African monsoon circulation (e.g., Parker et al., 2005; Flamant et al., 2009). Within the monsoon circulation the inner-tropical discontinuity (ITD)

separates the warm and dry Saharan air mass from the cooler (but still warm) and moist air mass of the monsoon flow originating from the Gulf of Guinea.

The monsoon circulation and thus the annual cycles of cloudiness and precipitation in the Sahel domain roughly follow the annual movement of the inter-tropical convergence zone (ITCZ). The ITCZ can be regarded as the band of maximum precipitation due to the largest atmospheric instability, also connected to the African Easterly Jet (AEJ) in the mid-troposphere. The ITD is the area of the strongest moisture gradient at surface level and represents the surface convergence zone of the Saharan and monsoonal air masses. The northern branch of the West-African Monsoon (WAM) sytem, i.e. the southward flow of hot, dry air from the Sahara, is often called Harmattan (e.g. N'Tchayi Mbourou et al., 1997). A more detailed description of the threedimensional flow patterns of the WAM system can be found in N'Tchayi Mbourou et al. (1997) and Lebel and Ali (2009).

The annual cycle of cloudiness and precipitation in the Sahel is characterised by the wet or monsoon season (rainy season), which accounts for most of the region's annual rainfall, followed by a long dry season characterised by only very little precipitation (N'Tchayi Mbourou et al., 1997; Klose et al., 2010). The wet season is during boreal summer, when the ITCZ reaches its northernmost position. Consequently the dry season lasts from boreal autumn to spring.

Aerosols interacting with the clouds connected to the West African monsoon are mainly mineral dust (either advected from the Sahara, e.g. Flamant et al., 2009, or emitted by local sources, e.g. Bou Karam et al., 2009), and soot aerosols originating form biomass burning and combustion (e.g. McConnell et al., 2008). Satellite-based case studies led to important improvements of our understanding of aerosols effects on cloud properties (e.g. Kaufman et al., 2002). Aerosols, including mineral dust, can act as cloud condensation nuclei (CCN), thus increasing the number of cloud droplets. Due to this increase of cloud droplets at reduced

droplet sizes the albedo of the cloud is increased (Twomey, 1974). Furthermore the small droplets decrease the precipitation efficiency of the clouds (Albrecht, 1989; Rosenfeld et al., 2001; Hui et al., 2008) and thus can change the cloud properties and extend their lifetime as the water may remain longer within the cloud (Haywood and Boucher, 2000; Stevens and Feingold, 2009). The increased cloud lifetime is reported to lead to increased cloud cover. In contrast to this "normal" behaviour in the case of generally low droplet sizes in the cloud field, the entrainment of giant condensation nuclei such as (aged) mineral dust particles also has been observed to be able to shift the cloud droplet size spectrum towards larger droplets (e.g. Feingold et al., 1999).

Moreover there are reports of a counteracting effect of absorbing aerosols: these lead to a stabilization of the atmosphere by solar heating of the aerosol layer (e.g. Kaufman and Fraser, 1997) and corresponding cooling of the surface due to the resulting lack of surface insolation (e.g. King et al., 1999; Klüser et al., 2008). These effects can cause a reduction of cloud cover (Perlwitz and Miller, 2010), which can counteract the cloud cover increase caused by the cloud lifetime effect. Klüser et al. (2008) also reported convective cloud formation due to large temperature gradients along sharp aerosol fronts as another pathway of cloud-aerosol-interaction. Especially in the case of mineral dust, the aerosols may also act as effective ice nuclei, initiating early freezing of cloud droplets and thus increasing cloud updrafts and cold-rain precipitation (DeMott et al., 2003; Jenkins et al., 2008), but there are also doubts if this effect is very common throughout Northern Africa (e.g. Ansmann et al., 2008).

Thus the net effect of aerosols on clouds and cloud properties remains uncertain due to several aerosol effects counteracting (Stevens and Feingold, 2009; Carslaw et al., 2010; Perlwitz and Miller, 2010). Moreover, also the chemical composition of the aerosol (aerosol type) might influence magnitude and even sign of the aerosol effect (Ramanathan et al., 2001; Perlwitz and Miller, 2010).

In order to separate the effects of different aerosol types on cloud properties there is a need for a differentiation of aerosol types in retrieved aerosol parameters. From observations of the MODerate resolution Imaging Spectroradiometer (MODIS) aerosol can be separated into coarse and fine mode (Hubanks et al., 2008).

The SYNergetic AErosol Retrieval SYNAER from ENVISAT observations (Holzer-Popp et al., 2008) is capable of aerosol type separation due to the exploitation of the synergy of a radiometer with good horizontal resolution (Advanced Along-Track Scanning Radiometer AATSR) and a spectrometer with coarse spatial but high spectral resolution (SCIAMACHY).

In contrast to most other aerosol species, mineral dust can also be detected in thermal infrared bands (Ackerman, 1997). Legrand et al. (2001) use brightness temperature differences between the observation day and the maximum of a prior two

weeks period for dust detection (Infrared Difference Dust Index, IDDI method) with Meteosat satellites of the first generation. Brindley and Ignatov (2006) and Li et al. (2007) present case studies of dust remote sensing form Meteosat Second Generation (MSG) thermal infrared bands. Klüser and Schepanski (2009) developed the Bitemporal Mineral Dust Index (BMDI), a method for dust detection with MSG Spinning Enhanced Visible and InfraRed Imager (SEVIRI) from a bi-temporal approach contrasting day and night time observations from two thermal infrared split window bands.

In this study the relationship between mineral dust aerosol and West-African monsoon cloudiness is analysed from five consecutive years of observations with three (plus one additional for season discrimination purposes) different satellites. Data and methods are presented in Sect. 2. Results of the statistical analysis are shown in Sect. 3 and discussed in Sect. 4. Finally, Sect. 5 summarises the results obtained in this study.

2 Data and methods

Data sources for this study are cloud and AOD observations (including dust separation) from MODIS, cloud, AOD and aerosol type observations from ENVISAT and as third satellite dataset cloud properties and BMDI mineral dust estimates from SEVIRI on Meteosat Second Generation (MSG). Moreover precipitation observations from the Tropical Rainfall Measuring Mission (TRMM) are used for determination of the monsoon and dry seasons (but not for analysis of aerosol cloud interactions).

Five consecutive years (2004–2008) of daily observations are analysed. MODIS observations (collection 005) are from the Aqua satellite, as the available Aqua data already include the "Deep Blue" aerosol retrieval over bright surfaces (Hsu et al., 2004) and provide observations in the "afternoon orbit", i.e. at local afternoon times (equator crossing time 13:30 local solar time [LST] in ascending orbit, thus covering the Sahel domain some minutes later). The MODIS atmosphere daily level 3 product (D3) combines aerosol and cloud observation averages at 1° resolution (Hubanks et al., 2008). Cloud observations used here include cloud cover, cloud top temperatures (CTT), cloud top ice phase fraction (IPF) and liquid clouds effective radius (R_e (l)) of the standard MODIS level 2 retrievals (King et al., 2003; Baum and Platnick, 2006).

Cloud top ice phase fraction is calculated from the MODIS data as the fraction of ice phase cloud cover (CC_{ice}) to total cloud cover (CC_{tot}):

$$IPF = 100\% \cdot \frac{CC_{ice}}{CC_{tot}} \qquad (1)$$

MODIS mineral dust aerosol type selection is done by the fine mode fraction η (part of the MODIS atmosphere products, Remer et al., 2006) in the case of the dark target product (standard MODIS collection 005 aerosol product). Instead

of separating aerosol optical depth (AOD) values into their coarse and fine mode fractions, scenes with $\eta < 0.5$ are assumed to represent dust conditions and scenes with $\eta > 0.5$ are assumed to represent fine mode conditions.

It has to be stated that Levy et al. (2010) reported the limited use of the fine mode fraction product in MODIS collection 005, as the retrieval tends to choose the dust type aerosol model also in the predominant presence of fine particles. Thus the correlation between MODIS derived η and fine mode fraction from AERONET is very weak and η does not represent the physical fraction of fine mode aerosol in the total aerosol burden. Nevertheless in this study cases clearly dominated by biomass burning aerosol shall be excluded from the analysis. As Levy et al. (2010) report a tendency of overestimating the dust fraction in the MODIS retrieval, the approach described above for the dark target product excludes observations very likely to show fine mode aerosol whereas the observations taken into account in the analysis still may include significant contributions of biomass burning aerosol. Moreover, as mineral dust and biomass burning aerosols themselves are mixtures of particles with different chemical composition, this approach seems to be better suitable for detecting relationships between mineral dust aerosol and cloud properties than the separation of AOD values (again see Levy et al., 2010).

For large parts of the analysis domain the dark target approach does not provide sufficient observations due to the high reflectance of the dry surface. Hsu et al. (2004) developed a method for remote sensing of aerosol with MODIS also over bright reflecting surfaces ("Deep Blue" method), for which the $0.412\,\mu m$ channel of the MODIS instrument is also exploited due to the higher contrast between aerosol and bright surfaces at this wavelength. For the MODIS "Deep Blue" observations, dust aerosol is characterised by AOD > 0.2 and Ångström exponent $\alpha < 0.6$. This method is motivated by Dubovik et al. (2002) who use a very similar approach for determining scenes which are very likely to show mineral dust. This dust separation method has also been used by Klüser and Schepanski (2009) where also a more detailed discussion of it can be found. MODIS observations as used here contain both retrieval results, dark target and "Deep Blue".

All MODIS observations are separated into three AOD classes (total AOD as retrieved by MODIS, dust filtering as described above, see Levy et al., 2010) where the first class represents dust free background conditions (AOD < 0.2), the second one indicates moderate dustiness (0.2 < AOD < 1.0, dust likely by filtering as above) and the third one is the class of high dust loadings (AOD > 1.0, dust likely by filtering as above). For each of the dust classes and for each cloud property to be analysed a histogram is then calculated which represents the observation density distribution. Statistical parameters of cloud properties are only calculated, if at least 100 cloud property observations are present for the respective AOD class.

The SYNergetic AErosol Retrieval SYNAER (Holzer-Popp et al., 2008) exploits synergies between the Advanced Along-Track Radiometer (AATSR) and the SCanning Imaging Absorption spectroMeter for Atmospheric CHartographY (SCIAMACHY) both operated on ENVISAT with an equator crossing time of 09:30 LST (morning orbit). AATSR provides good spatial resolution ($1 \times 1\,km^2$ at nadir), whereas SCIAMACHY provides a high spectral resolution at coarse spatial sampling ($60 \times 30\,km^2$ at nadir). The high spectral resolution of SCIAMACHY can be used for estimating aerosol speciation whereas the AOD of the given aerosol type is calculated from AATSR observations. Thus SYNAER retrieves not only AOD but also aerosol type. Only dust type aerosol observations of SYNAER are used here as dust AOD. Unlike MODIS observations, ENVISAT observations are separated in the subsets "background" (AOD < 0.2) and "dust" (AOD > 0.2, aerosol type dust), only: The reason for not separating into moderate and high dust loadings for ENVISAT observations is the lower sampling of SYNAER due to the coarse resolution, the repeat cycle of about 12 days at the equator and the limb-nadir alternation pattern of SCIAMACHY (Holzer-Popp et al., 2008).

Cloud properties from ENVISAT-AATSR observations are retrieved with the AVHRR Processing scheme Over Land, cLouds and Ocean (APOLLO) developed for the Advanced Very High Resolution Radiometer (AVHRR) by Saunders and Kriebel (1988), Kriebel et al. (1989) and Kriebel et al. (2003). Extensions to the standard APOLLO scheme for AATSR as described in Holzer-Popp et al. (2008) are also applied to the cloud observations here. Cloud top ice phase fraction is calculated with the phase discrimination algorithm and the "area weighted phase" method presented by Pavolonis and Heidinger (2004). ENVISAT observations are mapped onto a 1° grid.

SEVIRI cloud observations are compiled from cloud properties including cloud cover and CTT determined with the APOLLO scheme (as also used for ENVISAT-AATSR) in an adaptation to MSG observations. As for ENVISAT-AATSR, ice phase fraction is determined with the Pavolonis and Heidinger (2004) method. The presence of airborne mineral dust including a rough estimation of the dust load is obtained from SEVIRI observations with the BMDI method (Klüser and Schepanski, 2009). Day to night differences of brightness temperature in the $10.8\,\mu m$ band and of brightness temperature differences between the $12.0\,\mu m$ and the $10.8\,\mu m$ band are used to build this infrared dust index. As mineral dust absorption is stronger in the $10.8\,\mu m$ band than in the $12.0\,\mu m$ band and the presence of airborne dust reduces the diurnal contrast of $10.8\,\mu m$ brightness temperatures, low or negative BMDI values indicate high dust loads. The BMDI exploits the high contrast between day and night observations and thus depends on the highest possible contrast in surface temperature and also dust source activity. Thus it is not generally possible to exploit the full temporal resolution of SEVIRI with this method, but on the other hand BMDI is capable of

dust detection with SEVIRI over bright surfaces (Klüser and Schepanski, 2009). This results in the fixed observation time of the SEVIRI BMDI (and consequently also clouds) dataset of 12:00 UTC despite the general possibility of SEVIRI observations at other times of the day. The BMDI is not to be regarded as to be directly connected to dust AOD (see Klüser and Schepanski, 2009 for details of the BMDI evaluation), as it also depends on several other parameters such as the dust layer height, dust particle size and dust chemical composition. As presented in detail in Klüser and Schepanski (2009), correlation between AERONET (Holben et al., 1998) visible AOD (with the same dust filter as applied to MODIS observations in this study) and BMDI is $\rho = -0.792$, reflecting that low BMDI values represent higher dust loadings. As suggested in Klüser and Schepanski (2009) a dust detection threshold of 6 K is applied for BMDI observations. In order to have a continuous value range, MSG observations with clouds or dust-free scenes are set to this upper bound value (6 K), thus the data value range of BMDI observations is from 6 K (no dust observed) to −5 K (high dust load). BMDI is retrieved at the full spatial SEVIRI resolution ($3 \times 3 \, \text{km}^2$ at nadir).

Daily SEVIRI observations of clouds (APOLLO scheme) and airborne dust (BMDI), both retrieved at the full spatial SEVIRI resolution, are mapped onto a 0.5° grid for further analysis.

In contrast to solar range aerosol retrievals reliable dust detection with BMDI is limited to scenes with low water vapour due to water vapour absorption in the thermal infrared. BMDI observations are generally possible for water vapour columns (WVC) lower than 6 cm (Klüser and Schepanski, 2009). In order to be comparable to the other datasets used here, an even lower threshold of WVC < 3 cm (obtained from the MODIS WVC product) has been applied to the SEVIRI dataset. The 3 cm threshold is also used for separation of moist and dry air masses within the monsoon regime of West Africa throughout this study. Thus only dust and clouds in the dry branch of the monsoon circulation (Harmattan regime) are considered in SEVIRI data.

Again, BMDI analyses are separated into the three classes "no dust" (BMDI ≥ 6 K), "moderate dust" (6 K > BMDI ≥ 0 K) and "high dust" (BMDI < 0 K). Then, histograms for cloud properties are calculated as described above for these three BMDI dust classes.

In order to sample similar meteorological conditions (at least with respect to the moisture supply for cloud development), the aerosol and cloud observations of all satellite datasets are separated into a moist and dry air mass. In the Sahel the ITD builds a quite sharp moisture gradient, but the three-dimensional circulation limits the validity of the surface moisture gradient and wind field as a proper air mass separator (N'Tchayi Mbourou et al., 1997; Parker et al., 2005; Klose et al., 2010). Especially as long as the aerosol observations are not height resolved (as is the case for all satellite products used here), air mass separation should also
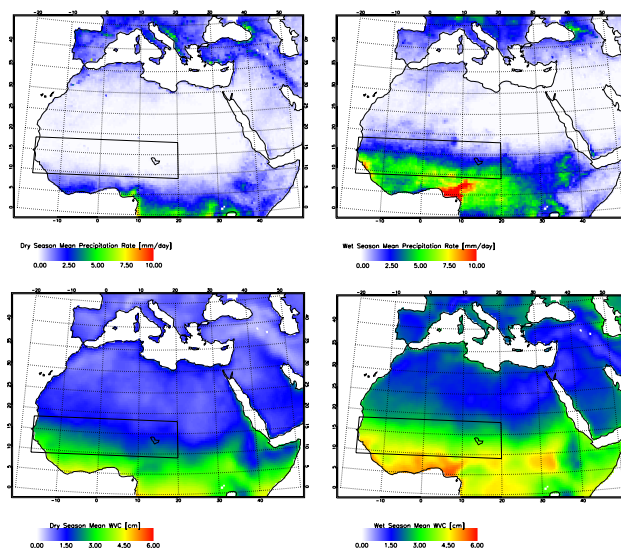

Fig. 1. Mean daily precipitation from TRMM observations 2004–2008 (top line) and corresponding MODIS Water vapour Column (bottom line) in Northern Africa for the dry (left row) and wet (right row) seasons. The black boxes highlight the Sahel domain.

be done without respect to one specific height level in order to avoid misinterpretations of the results (see Klose et al., 2010). The MODIS water vapour column (WVC) product (vertically integrated water vapour) is used here as and indicator of the air masses. Also the BMDI evaluation has been performed with this product (Klüser and Schepanski, 2009). As already presented in the description of the BMDI dataset, a separation value of WVC = 3 cm is used, where lower WVC indicates dry air mass corresponding to the Harmattan flow and higher WVC indicates moist air mass connected to the monsoon flow. The WVC should be regarded as an air mass separator, but not as a true separator of the near surface flow, as e.g. the ITD is. Mean WVC for Northern Africa of the Sahelian dry and wet seasons is presented in Fig. 1. It is clearly evident that the dry air mass is predominant in the Sahel region (9° N–18° N, 17° W–20° E; black boxes in Fig. 1) during the dry season, when the moist air mass is present in the Southernmost part of the domain. During the wet season the moist air mass is predominant and the dry air mass is confined mainly to the Northern part of the region. Nevertheless there are large variations of air mass intrusion towards the North or South in the region throughout both seasons (see e.g. Knippertz and Fink, 2006).

Precipitation observations are taken from the TRMM 3B42 product, where three-hourly rain rates are generated from a combination of infrared observations of geostationary satellites and TRMM passive microwave and radar observations (Huffman et al., 2001, 2007). The mean daily precipitation rates of the dry and wet seasons observed by TRMM for the years 2004–2008 are also depicted in Fig. 1. The monsoon cycle with hardly any precipitation in the Sahel during
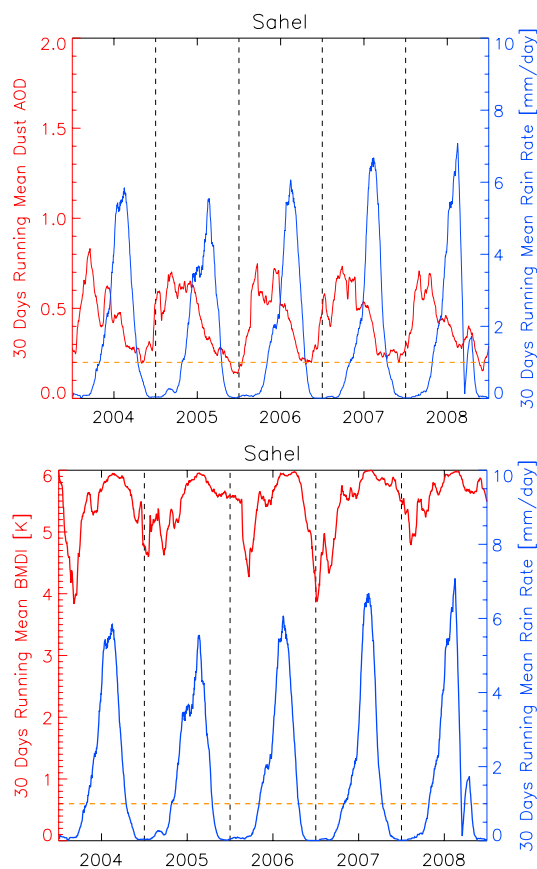
Fig. 2. Sahel daily rain rates (30 day running mean, blue) and mineral dust AOD from MODIS (top) and BMDI (bottom) (30 days running mean, red) time series for the years 2004–2008. The horizontal dashed lines are the 1 mm/day rain rate threshold to separate monsoon and dry seasons.

the dry season and far-north reaching monsoon rainfall during the wet season can clearly be seen.

TRMM data are only used for determining wet and dry seasons (of the West-African Monsoon system). Effects of mineral dust on precipitation are not studied here. This study investigates only the change cloud properties under the presence of dust, which is observed from the same satellites (and the same instruments) and at the same time as the dust observations.

The West-African monsoon season is often determined solely by including a fixed period in the analysis (see e.g. N'Tchayi Mbourou et al., 1997 for different monthly definitions of the monsoon season in the Sahel). This approach does not seem optimal in order to analyse aerosol effects on West African monsoon clouds as its onset depends on a number of other factors and varies significantly from year to year. If analysing a fixed period the data could easily include a number of pre- or post-monsoon days for a delayed or very early monsoon onset. In this study the monsoon season is therefore determined directly form rainfall observations of
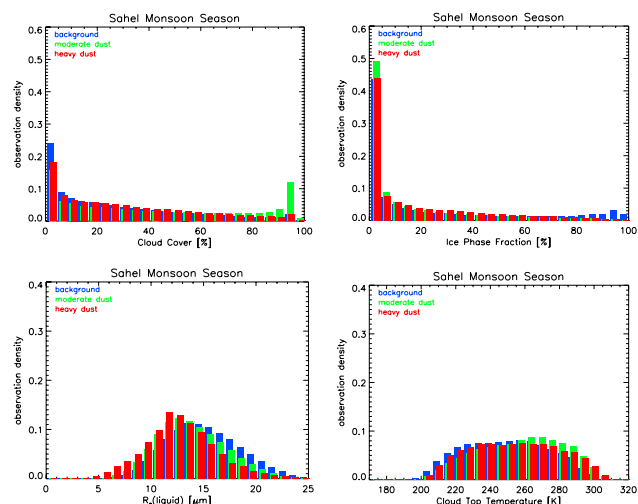

Fig. 3. Histograms of MODIS cloud cover (top left), ice phase fraction (top right), liquid cloud effective radii (bottom left) and cloud top temperature (bottom right) for no, moderate and heavy mineral dust AOD load (blue, green and red, respectively). These histograms show the shape of the overall distributions during the wet (monsoon) season and are not separated by air mass.

the TRMM 3B42 product (TRMM observations hereafter). In order to derive the monsoon season daily TRMM precipitation sums are averaged over the whole Sahel domain and from those daily Sahel rainfall averages a 30 days running mean is generated. Days with 30 days running mean rainfall larger than 1 mm/day are regarded as monsoon days, all other days belong to the dry season. Figure 2 shows the 30 days running mean of precipitation together with the respective seasonal cycles of average dust AOD (from MODIS) and average BMDI over the Sahel domain. The 1 mm threshold is indicated by the dashed lines indicating the good representation of the seasonal cycle by this method. It is obvious that MODIS dust AOD and BMDI, although both are used as indicators of dust activity, are not perfectly well (anti-) correlated. Klüser and Schepanksi (2009) discuss the differences between MODIS dust AOD and BMDI in detail, they are mainly due to the different retrieval methods (reflected solar versus thermal infrared radiation, radiative transfer retrieval versus BTD index) and moreover to the fact that BMDI is also influenced by the dust layer height and also the surface emissivity – and not by biomass burning aerosol contributions to the total aerosol load in the Sahel (McConnell et al., 2008; Klüser and Schepanski, 2009).

3 Results

3.1 MODIS dust and cloud observations

Histograms of the observations densities of cloud cover, cloud top ice phase fraction, liquid cloud effective radius and

Table 1. Numbers of observations (# obs) within the respective subsets for the three different satellite datasets, separated by season (all) and air mass (MODIS and SEVIRI).

dataset	season	air mass	dust load	# obs
MODIS	dry	dry	background	448 218
			moderate	370 758
			heavy	75 211
		moist	background	108 545
			moderate	95 950
			heavy	9680
	wet	dry	background	241 454
			moderate	145 603
			heavy	32 152
		moist	background	312 721
			moderate	242 826
			heavy	22 468
ENVISAT	dry	–	background	879
			dust	153
	wet	–	background	2103
			dust	343
SEVIRI	dry	dry	background	69 646
			moderate	11 571
			heavy	499
	wet	dry	background	129 450
			moderate	1789
			heavy	86

Fig. 4. Observation density differences of MODIS cloud top temperature for moderate (left) and heavy dust (right) classes and different flow regimes (air masses) during the wet (blue) and dry (red) season.

cloud top temperature (CTT) from Aqua MODIS are presented in Fig. 3 for the three classes of dust aerosol load (as obtained from MODIS observations) during the Sahelian wet season. The corresponding numbers of observations for each subset are provided in Table 1. It is clearly evident that the background class is the most often observed one and that moderate dust conditions are more often observed than heavy dust conditions (in all subsets). Moreover it is clear that the MODIS dataset by far provides the highest number of observation points compared to the ENVISAT and SEVIRI datasets.

The cloud cover histograms show only the observation density for cloudy pixels, thus totally cloud free scenes are excluded from this histogram in order to pronounce the effects observed in the presence of clouds. Moreover the samples of the other cloud property histograms also include only the cloudy scenes, thus with this approach the database of all four histograms shown in Fig. 3 is exactly the same.

Generally it is evident that very high cloud cover is more frequent in the presence of airborne dust than for the background. On the other hand very low cloud cover observation densities are decreased for the moderate and heavy dust classes compared to the background observations.

CTT observation density distributions show an indication of relationships between mineral dust and monsoon cloudi-
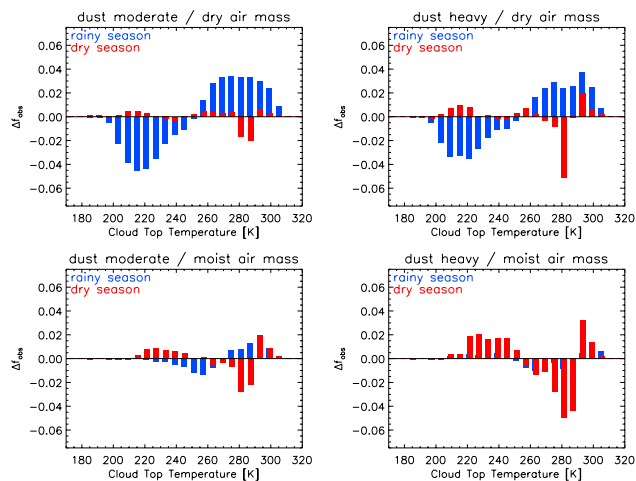
ness. For dusty scenes the histograms are shifted towards higher CTT. Under the presence of moderate dust loads the primary peak of the histogram representing shallow warm top clouds (CTT > 270 K) becomes more pronounced on the expense of the higher clouds (colder cloud tops). For heavy dust the shift towards higher CTT is even more pronounced than for moderate dust, but the shape of the histogram (fractions of primary and secondary peak) is much more similar to the background conditions than for moderate dust.

A more detailed analysis is performed from the MODIS observations, taking into account the air mass of observations, as it represents different meteorological conditions for cloud formation and development. The ITD divides the moist monsoonal flow from the hot and dry Harmattan flow (see e.g. Tulet et al., 2008). MODIS water vapour column (WVC) observations are used to identify the air mass regime. WVC larger than 3 cm is assumed to represent the moist air mass (of the monsoonal flow) whereas the dry air mass (Harmattan flow) is attributed by WVC < 3 cm (see also Klüser and Schepanski, 2009). Differences in observation density f_{obs} defined as

$$\Delta f_{obs}(\text{moderate dust}) = f_{obs}(\text{moderate dust}) - f_{obs}(\text{background})$$
$$\Delta f_{obs}(\text{heavy dust}) = f_{obs}(\text{heavy dust}) - f_{obs}(\text{background})$$

(2)

are presented for cloud top temperature (Fig. 4) and liquid phase effective radius (Fig. 5) for both, dry and moist air masses and for both seasons.

Figure 4 presents cloud top temperature observation density differences as observed from MODIS under different dust conditions. Within the dry air mass CTT distribution differences with respect to dust presence are larger in the monsoon season than in the dry season. In the moist air mass it is vice versa. Under dusty conditions in the dry air mass of
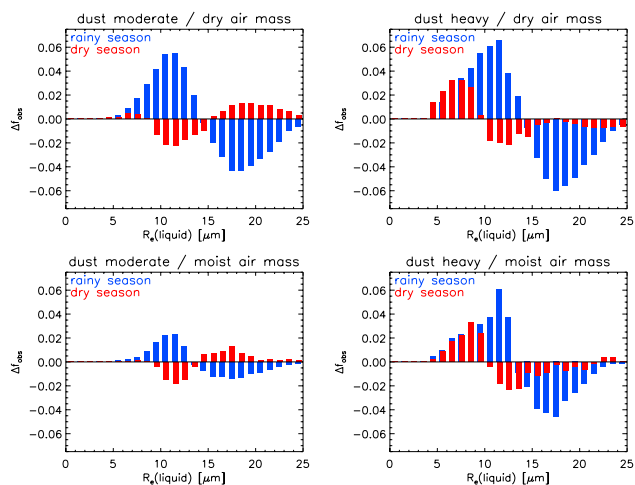
Fig. 5. Observation density differences of MODIS liquid cloud effective radius for moderate (left) and heavy dust (right) classes and different flow regimes (air masses) during the wet (blue) and dry (red) season.

Fig. 6. Histograms of ENVISAT cloud cover (top line) and cloud top temperature (bottom line) for the Sahelian dry (left row) and wet (right row) seasons, separated into background and dust observations.

the monsoon season an increase in cloud top temperature is observed. During the dry season's dry (Harmattan) air mass a small increase of very low CTT (<220 K) is evident. Also the observation densities of mid-level clouds are slightly increased whereas the probability of low level clouds is somewhat reduced. The same holds for the moist air mass of the dry season. Furthermore, within the moist air mass of the monsoon season the same effect takes place as for the dry air mass, i.e. an increase in CTT, but with much smaller magnitude.

Liquid phase cloud effective radii, representing droplet sizes of the liquid fraction of the total cloudiness, are analysed in Fig. 5 for the different seasons and air masses. Again the differences with respect to dust activity are stronger within the dry Harmattan air mass than in the moist air mass, but this changes from season to season. During the monsoon season R_e (liquid) is much lower when also airborne mineral dust is observed, mainly within the dry air mass but also within the moist one. Large liquid phase droplet sizes become very infrequent, as is evident from Fig. 3. During the dry season under moderate dust loadings an opposite effect on liquid phase cloud effective radius is evident: effective radii are increased with respect to dustiness in both, dry and moist air mass. Under heavy dust loads within both flows of the dry season cloud effective radii are reduced again.

3.2 ENVISAT dust and cloud observations

Despite the lower sampling ENVISAT observations provide a direct aerosol type separation (Holzer-Popp et al., 2008). On the other hand the cloud properties obtained from AATSR observations lack an effective radius retrieval in the APOLLO method (Kriebel et al., 2003). Neverthe-
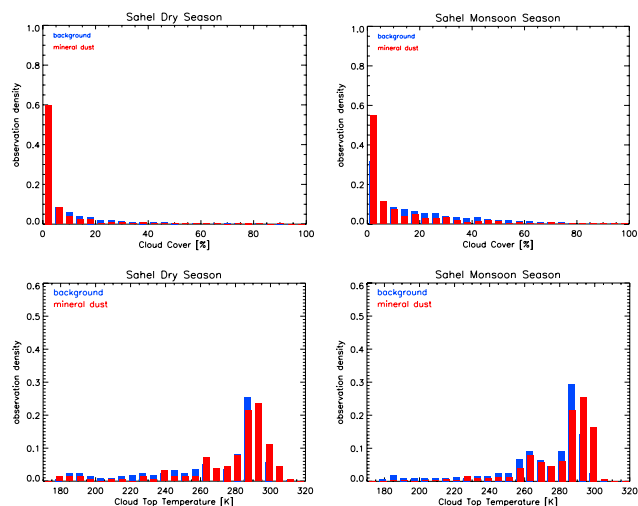
less the same analysis as for MODIS can be performed from the ENVISAT observations. Due to the lower sampling no air mass separation is performed for ENVISAT observations and observations are only separated into two dust classes: background (AOD < 0.2) and dust (AOD > 0.2, aerosol type "dust"). As no such method as Deep Blue is exploited within SYNAER, aerosol retrieval is only possible, if a sufficient number of AATSR dark fields are found within a SCIA-MACHY pixel (Holzer-Popp et al., 2008). Thus ENVISAT observations are mainly from the vegetated areas of the Sahel, which follow the shift of the ITCZ during the course of the year (with some delay). The much lower sampling (compared to MODIS) is evident from the observation numbers presented in Table 1. Interestingly, due to the higher vegetation cover needed for the AATSR dark field detection, the number of observations is higher in the cloudy monsoon season than in the dry season, when less clouds are present in the Sahel.

Histograms of cloud cover and cloud top temperature for background and dust observations from ENVISAT are presented in Fig. 6. Again, cloud cover presented in Fig. 6 is total cloud cover of all (partly) cloudy grid boxes. As all other cloud parameters are only retrieved in the case of cloudy scenes, the samples of the cloud cover and cloud top temperature histograms are exactly the same. It is evident that cloud cover is reduced under the influence of mineral dust in both seasons in the Sahel. Also the changes of the cloud top temperature histograms with dust activity (from ENVISAT observations) look similar in both seasons: a reduction of high and mid-level clouds (cloud top temperatures below 270 K) is accompanied by an increase of the shallow liquid phase fraction (CTT > 270 K). Especially in the monsoon season the
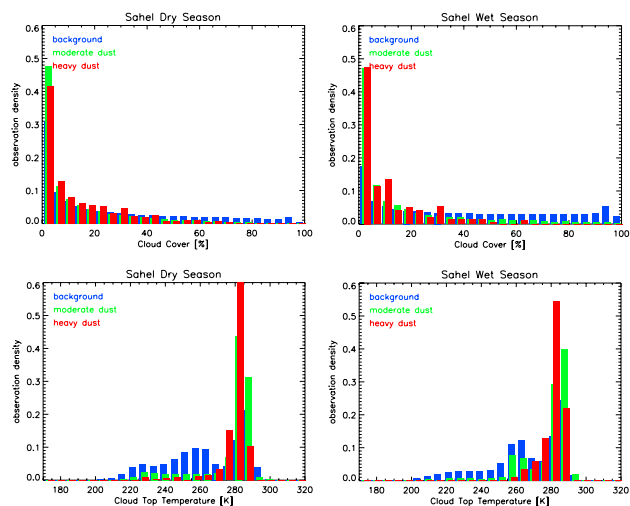
Fig. 7. Histograms of SEVIRI cloud cover (top row) and cloud top temperature (bottom row) observed at 12:00 UTC for three BMDI dust classes (colours as in Fig. 3) in the dry and wet seasons (left and right, respectively; dry air masses only).

secondary peak of mid-level clouds in the histogram is weakened under dust influence whereas very warm cloud tops are more often observed than in the background case. Ice phase fraction is reduced under dusty conditions in good agreement with the CTT observations (not shown), thus it is likely that the observed IPF decrease is rather due to the higher fraction of shallow clouds than to ice nucleation effects of the dust aerosol. Cloud effective radius is not retrieved with the APOLLO method.

3.3 SEVIRI dust and cloud observations

Similar analyses as for MODIS and ENVISAT have been performed from SEVIRI BMDI and cloud observations. Again, histograms are calculated separately for the three classes "no dust" (BMDI ≥ 6 K), "moderate dust (0 K $<$ BMDI ≤ 6 K) and "heavy dust (BMDI < 0 K) and are presented in Fig. 7 for cloud cover and CTT. Being an infrared estimate of the airborne dust load, BMDI is also sensitive to the dust layer height, thus lower BMDI values could also correspond to moderate optical depths but at higher altitudes (see discussion in Klüser and Schepanski, 2009). Moreover, BMDI is only capable of dust detection in dry environments as water vapour absorption at 11 μm influences the brightness temperature difference approach used. Thus only BMDI and SEVIRI cloud observations of the dry Harmattan air mass (MODIS WVC < 3 cm) are used here. Observation numbers are still sufficient for statistical analysis, but the heavy dust class within the wet season clearly has a lack of observations compared to the others.

High cloud cover values are much less likely when moderate and high dust is observed with BMDI. The observation density distributions of cloud top temperatures in both

seasons have a different shape than those of MODIS. Shallow clouds are much more represented and mid-level clouds (CTT between 250 K and 270 K) show a distinct secondary peak in the distributions of all three dust classes. Under heavy dust loads within the Harmattan flow most clouds present are shallow cumulus clouds, the observation frequency of mid-level clouds is strongly reduced.

The ice phase fraction is significantly reduced in dust scenes corresponding to a strong increase in CTT (not shown). The shallow clouds representing the majority of cloud observations in heavy dust cases have CTTs mainly well above the freezing level, thus water phase is much more pronounced. As no effective radii are retrieved from SEVIRI observations with APOLLO, the relationship between dust and droplet sizes cannot be discussed here in detail.

3.4 Observed net cloud property changes

The differences in observation densities, Δf_{obs} as defined in Eq. (2), are used to calculate the overall cloud cover changes in the presence of dust for two dust classes, for both seasons and for both flow regimes (air masses), separately.

The overall cloud property change, denoted as δ_{obs} here for the cloud parameter "obs", is calculated as

$$\delta_{obs} = \sum_{i=1}^{N_{bins}} obs_i \cdot \Delta f_{obs}(i) \qquad (3)$$

where obs_i is the parameter value of the i-th histogram bin and N_{bins} the number of bins in the histogram ($N_{bins} = 25$ for all datasets). δ_{obs} is evaluated for both dust load classes separately (MODIS and SEVIRI only). These instantaneous overall cloud property changes as found in the observations of the three satellite datasets are presented in Table 2, separated by air mass (MODIS and SEVIRI) and season (all).

From the MODIS numbers given in Table 2 it is clearly evident that the cloud microphysics are subject to strongest changes with respect to dust activity within the dry air mass of the monsoon season. This is also supported by the SEVIRI observations whereas for the ENVISAT data no air mass separation has been performed. In this season and air mass cloud cover is drastically reduced for the dust classes and CTT is increased by more than 10 K. The ice phase fraction is also significantly reduced, which is in clear correspondence to the increased CTT (reduced cloud top height).

MODIS observations show a strong reduction of liquid phase (and ice phase, not shown) cloud effective radii (no R_e retrieval from ENVISAT and SEVIRI) in most subsets, only moderate dust loads within both air masses of the dry seasons are connected to an increase in effective radius (indicating an increased droplet size).

Besides the instantaneous cloud property changes observed within the respective subsets of all observations, these values have been used to estimate the overall mean change throughout the observation time. The instantaneous cloud

Table 2. Instantaneous change of cloud cover (δ_{COV}), cloud top temperature (δ_{CTT}), ice phase fraction (δ_{IPF}) and liquid phase effective radius ($\delta_{R_e \text{ (liquid)}}$, MODIS only) in the presence of dust as observed from the three different satellite datasets, separated by season (all) and air mass (MODIS and SEVIRI).

dataset	season	air mass	dust load	δ_{COV}	δ_{CTT}	δ_{IPF}	$\delta_{R_e \text{ (l)}}$
MODIS	dry	dry	moderate	−1.65%	−1.13 K	−0.90%	+0.62 µm
			heavy	+2.06%	−1.49 K	−1.53%	−1.14 µm
		moist	moderate	+0.53%	−1.22 K	−1.04%	+0.32 µm
			heavy	+6.99%	−4.06 K	+1.29%	−0.64 µm
	wet	dry	moderate	−20.84%	+14.07 K	−16.90%	−2.39 µm
			heavy	−14.73%	+12.06 K	−14.15%	−3.16 µm
		moist	moderate	−0.66%	+2.51 K	−1.04%	−0.73 µm
			heavy	+5.12%	−0.55 K	+2.03%	−1.91 µm
ENVISAT	dry	–	–	−1.42%	+8.40 K	−8.23%	–
	wet	–	–	−7.60%	+11.16 K	−6.00%	–
SEVIRI	dry	dry	moderate	−6.65%	+13.93 K	−11.22%	–
			heavy	−5.90%	+15.89 K	−15.70%	–
	wet	dry	moderate	−21.31%	+12.37 K	−15.78%	–
			heavy	−21.68%	+14.89 K	−22.88%	–

Table 3. Mean cloud property changes in the presence of dust, averaged with appropriate weighting of occurrence, throughout the years 2004–2008 as observed by the three different satellites.

dataset	δ_{COV}	δ_{CTT}	δ_{IPF}	$\delta_{R_e \text{ (liquid)}}$
MODIS	−3.27%	+2.06 K	−3.12%	−0.45µm
ENVISAT	−3.50%	+9.33 K	−7.48%	–
SEVIRI	−17.49%	+12.80 K	−15.07%	–

property changes have been weighted with the appropriate frequency of occurrence of air mass and season and thus have been merged into one number per cloud observable for each satellite dataset. The mean changes from all three satellite datasets are given in Table 3. Unlike for the instantaneous cloud property changes the three satellite datasets show the same sign of mean changes for all cloud observables in the Sahel domain. But the magnitudes still show large differences. The mean cloud cover changes observed with MODIS and with ENVISAT are quite similar, whereas the cloud top temperature change (higher CTT: lower cloud tops) is much stronger from ENVISAT than from MODIS. As R_e (liquid) is only retrieved from MODIS, no comparison is possible, but at least the net change of effective radius observed by MODIS points into the expected direction: lower effective radius under dust influence than for the background. The CTT and IPF changes are similar between SEVIRI and ENVISAT observations, whereas the SEVIRI observed net cloud cover change is much stronger than from the other datasets. If the numbers of Table 3 are compared with

those of Table 2 it becomes obvious that a large variety of different observed differences between dust scenes and background form the basis of the net changes. It is evident that the observed cloud property changes differ from air mass to air mass and from season to season.

3.5 Regional distribution of observed net cloud property changes

In order to give an estimation of the spatial patterns of the observed cloud property changes connected to activity of airborne dust, maps of the net cloud property change (calculated as exactly the same property as in Eq. (3)) have been generated for Northern Africa. These are presented in Fig. 8 for cloud cover and cloud top temperature changes for dry and wet seasons (of the Sahel, although the seasons may differ in other parts of the maps). The cloud property changes have been calculated for each grid box from MODIS observations (dataset with the highest number of available observations) for the moist and the dry air mass within the season separately and both values have been averaged appropriately (weighted with the fraction of each subset in the total grid box observations). Grid cells with less than 100 observations for each, background and airborne dust, are treated as missing data. The number of missing grid cells in the Sahel domain (highlighted as black boxes) is small during both seasons and mainly concentrated around the Lake Chad/Bodélé Depression region in the North-Eastern corner of the domain (due to a low number of background observations connected to very frequent dust activity; see also Klüser and Schepanski, 2009).
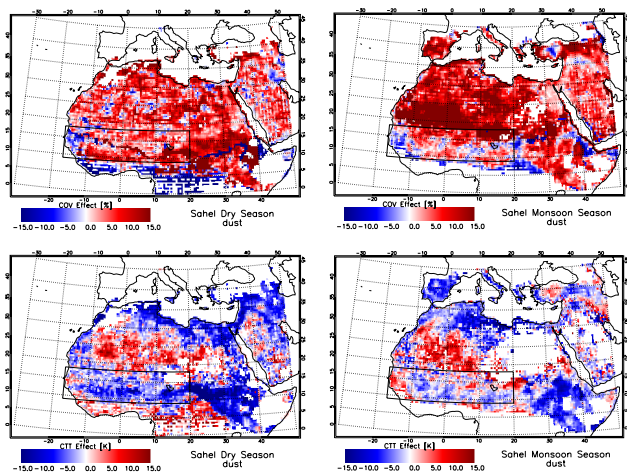
Fig. 8. Spatial distribution of mean changes of cloud cover (top row) and cloud top temperature (bottom row) with dust activity seasonally separated into Sahelian dry (left) and monsoon (right) season as observed from MODIS.

During the dry season cloud cover is mainly increased in the presence of mineral dust, but in the Western parts of the domain (Sahel domain again indicated by the black boxes in the maps) there are also some grid cells showing cloud cover net decrease in dust presence. Accordingly cloud top temperature is mainly decreased during the Sahelian dry season when dust is observed. This decrease is strongest in the Central Sahel.

During the monsoon season the cloud cover is also increased connected to dust activity in the Northern and Southern parts of the Sahel domain and some cloud cover decrease can be observed in between. The cloud cover reduction is stronger in the Western part of the domain than in the Eastern part. The picture for monsoon season cloud top temperature change is somewhat more complex with both decrease and increase being present around the domain. The strongest increase in CTT with dust activity is observed along the domain's West coast and another strong CTT increase is evident for the North-Eastern part of the domain.

The sample sizes of the ENVISAT and SEVIRI datasets are not sufficient for similar analyses, thus spatial distributions of the observed cloud property changes are only presented for MODIS.

4 Discussion

Most aerosol-cloud interaction studies concentrate on shortwave radiative effects due to changes in cloud cover and cloud albedo (e.g. Twomey, 1974; Kaufman and Fraser, 1997). Many of the aerosol-cloud interaction studies referred to in the introduction focus on pollution or biomass burning aerosol, i.e. fine mode aerosol particles. The effects of mineral dust aerosol covering the whole size range from fine to

coarse and giant mode particles are a combination of microphysical (e.g. droplet size reduction), thermodynamical (availability of suitable ice nuclei, solar heating) and meteorological (entrainment of dry warm air, stabilisation of the boundary layer and surface cooling) effects as indicated by the results shown here as well as by previous case studies and numerical modelling experiments.

As is clearly evident from the presented histograms, especially those of cloud top temperature, the samples of MODIS, ENVISAT and SEVIRI observations do not cover exactly the same atmospheric conditions (besides differences in the retrieval methods). While for ENVISAT a high observation density of shallow clouds accompanied by a distinct secondary peak of mid level clouds and low observation numbers of cold top clouds are present (similar to the SEVIRI background sample), the MODIS CTT histograms are much broader and do not show a strong bi-modality. Several effects can be addressed to be responsible for these differences. One issue is the size of the single footprint. While it is much finer for the MODIS retrievals, the SYNAER retrieval resolution is bound to the SCIAMACHY pixel size ($60 \times 30\,km^2$ at nadir). The necessity of such pixel being cloud free to a large amount (at least 50%, see Holzer-Popp et al., 2008) together with the need of the presence of dark surfaces within the SCIAMACHY pixel act as strong boundary conditions for the aerosol retrieval, which are not as tight for the MODIS products (better spatial resolution, retrieval also over bright surfaces with the Deep Blue method). But these are not the only differences. Also the observation times lead to different cloud conditions as the Sahel cloud state is characterised by a strong diurnal cycle. ENVISAT overpasses are in the morning hours (around 09:30 LST), whereas the Aqua overpasses are around 13:30 LST. Unfortunately no Deep Blue observations are available from Terra for the observation period, thus morning orbit MODIS observations cannot be used in this context. The difference of observation times means that in the ENVISAT observations the strongly pronounced shallow cloud (warm top clouds) peak together with the weaker secondary peak of mid-level clouds and less observations of cold top clouds represent the onset of the actual day's convective cycle. In the afternoon hours of the Aqua-MODIS observations a larger fraction of these convective clouds has already grown larger, thus the histogram is shaped more smoothly. The SEVIRI cloud observations, of 12:00 UTC, are located between the ENVISAT and the MODIS observations. But they are limited to the dry air mass and to cloud free conditions at both, night and day observation times. Furthermore, BMDI dust observations are height dependent and dust very close to the surface is not observed at all with thermal infrared methods. These strong constrains explain the very strong predominance of the shallow cloud peak in the SEVIRI histograms – and thus also (partly) the strong negative cloud cover change and positive cloud top temperature change observed from the SEVIRI dataset.

In contrast to SEVIRI, MODIS and ENVISAT aerosol observations are independent of aerosol layer height and also are capable of near surface dust observation. Another source for differences could be the sensitivity of MODIS to other aerosol species such as from biomass burning. McConnell et al. (2008) describe observations of vertically separated aerosol layers of mineral dust and biomass burning aerosol during the Sahelian dry season. During the dry season they observe mineral dust often to be transported below the biomass burning plume and thus near the surface, where the sensitivity of BMDI reaches its limits. Moreover, the cloud property changes observed by MODIS are most often the sum of dust and maybe contributions of biomass burning aerosols (see Levy et al., 2010). The same is partly true for the ENVSIAT observations, although the direct aerosol type classification restricts the observations to cases where mineral dust by large dominates the total aerosol. The classification of mineral dust by BMDI on the other hand is only sensitive to mineral dust, but at the prize to be sensitive to the height of the dust plume.

The different observation times and sensitivities to aerosol type do not explain all differences between the three satellite datasets, but they should be taken into account when interpreting the results – as well as the fact that all three datasets have different strengths and limitations and thus do not sample the same (meteorological) conditions.

Moreover it is clear from the principles of passive remote sensing of clouds and aerosols that e.g. dust below clouds (such as e.g. arcus clouds connected to haboobs) cannot be observed with these methods. Thus the results shown here may underestimate the dust activity caused by cold-pool outflows. Also dust above shallow clouds, which is not recognised as such by the cloud retrievals, might affect the results as in this case both, dust class and cloud properties would have larger errors. These limitations cannot be resolved with traditional methods of passive remote sensing of clouds and aerosol as used here. But nevertheless as we use only large-scale statistical analysis for the interpretation, the differences between dusty conditions and background conditions seem to be large enough in most cases to allow for interpretation of the results as interactions between dust and clouds – especially as previous (case and modelling) studies provided sufficient evidence of indirect aerosol effects for explaining the cloud property changes observed in the datasets used here.

MODIS observations mainly show a strong reduction of liquid cloud effective radii under mineral dust activity, as expected from the results of various previous studies on aerosol cloud interactions (see e.g. Ramanathan et al., 2001). But also cases with effective radius increase under dusty conditions are observed in the dry season (at moderate dust loadings within the dry air mass). The increase of effective radii for moderate dust load of the dry season might be the result of the combination of generally smaller effective radii in the dry season's non-precipitating clouds and the large dust particle acting as giant CCN (GCCN) directly initiating the formation of large cloud droplets, an effect already described by Feingold et al. (1999) from case study results. As no in-situ observations are available for this kind of analysis and as the MODIS dataset is the only one to include effective radius retrieval, this mechanism remains somewhat speculative, but the effective radius increase at least is evident from the statistical analysis.

The observed increases in cloud top temperature (MODIS dry season, ENVISAT, SEVIRI) are corresponding to reductions of cloud cover and can be explained by suppression of initial convection by stabilisation of the atmospheric layer. The atmospheric stability can be increased by absorbing aerosols due to a warming of the layer itself and an accompanying cooling (respective reduced warming, see King et al., 1999) of the surface. This stabilisation effect, being reported from observations of soot aerosol in Amazonia (Kaufman and Fraser, 1997), dense oil fire plumes over the Middle-East (Rudich et al., 2003) and also for dust aerosol from numerical modelling (Perlwitz and Miller, 2010), gives evidence that dust activity in the Sahel affects convective intensity and activity within the region (see also Perlwitz and Miller, 2010). The change of the ice phase fraction with dust activity is mostly connected to the CTT change (decrease of IPF with CTT increase and vice versa), thus it is not really evident from these observations, whether the dust particles act as effective ice nuclei or not. The only cases where this correlation between CTT and IPF is not present are cases with negative CTT change and also negative IPF change under the presence of mineral dust. Thus these do also not indicate a strong IN capability of the dust (see also Ansmann et al., 2008).

From the histogram analysis it follows that the mean cloud property changes do not show the total spectrum of changes of cloud property observation (or probability) density. For example in the moist air mass of the dry season, the net cloud top temperature change observed by MODIS is -1.22 K for moderate dustiness and -4.06 K for heavy dust loads. The histogram changes (Fig. 4) show that the rise of the cold top cloud occurrence (CTT < 250 K), which is mainly responsible for the observed net reduction, is accompanied by a decrease of clouds with CTT between 250 K and 290 K, but another increase of observation density for clouds with very warm tops (CTT > 290 K).

Generally from MODIS a decrease of cloud top temperature with dust activity is observed in the dry season whereas an increase is found in the wet season. In all cases but the dry air mass of the dry season (with moderate dust load) CTT decreases are accompanied by cloud cover increases and vice versa. The same is also observed from both other satellite datasets (from these only CTT increases and cloud cover decreases are observed).

The CTT decrease with corresponding cloud cover increase gives evidence for the presence of the cloud lifetime effect under favourable, but not all conditions – especially

as it is mainly observed together with cloud effective radius reductions.

The ENVISAT cloud cover histograms (Fig. 6) show that generally low cloud cover conditions are much more dominant in the ENVISAT observations than in the MODIS observations. Under the influence of mineral dust, the cloud cover is even more reduced (or dust is observed under lower cloud cover conditions). Correspondingly the observation density of warm top clouds is more pronounced with presence of airborne dust whereas frequency of cold top clouds is even more reduced. The effects are similar for both seasons. This is an indication for similar meteorological conditions being sampled with ENVISAT in both seasons, which limits the ENVISAT observations to favourable conditions (also surface vegetation). Nevertheless also under these limited conditions the effect of convective suppression (likely due to the atmospheric stabilisation rather than to microphysical in-cloud effects) is clearly evident from the observations. The reduction of cold top and mid-level clouds together with the increase of observations of very warm top clouds under the presence of airborne dust leads to such strong positive net CTT change compared to MODIS at comparable net cloud cover changes (Table 2).

For the BMDI dust classes a reduction of convective intensity with increasing dust load is observed in both seasons (Fig. 7). Under heavy dust conditions no CTT decrease is observed with BMDI. The warm and dry Harmattan air suppresses convective activity and thus a possible relationship between dust and CTT might be outweighed by semi-direct effects, which cannot be resolved from this kind of statistical analysis.

The mean cloud cover changes in the presence of dust, averaged with appropriate weighting of the occurrence frequency, indicate a predominance of the convection suppression effect over the cloud lifetime effect in the Sahel domain (Table 3). The signs for cloud cover, cloud top temperature and ice phase fraction change are equal from all three satellite datasets, whereas the magnitudes differ a lot. Effective radius is only retrieved from MODIS observations, the mean net change is negative, as would be expected form the large amount of previous studies. While MODIS and ENVISAT show a similar cloud cover reduction of -3.27% and -3.50%, respectively, it is much stronger from the SEVIRI observations – mainly due to the restrictions of the BMDI method (as discussed above).

From the spatial distribution of averaged net cloud property changes connected to dust activity (as obtained from MODIS observations) over Northern Africa (including the Sahel and adjacent regions) it is evident that in the Sahel cloud cover change and cloud top temperature change are mainly connected to each other, but not perfectly correlated (as is also evident from the detailed MODIS analysis as summarised in Table 2). During the dry season cloud cover increases in the Sahel are well correlated to cloud top temperature reductions, as already indicated by the histogram analy-

sis. The strongest cloud cover increase (in the Central Sahel) thus is tightly connected also to the strongest CTT reduction, whereas the area of cloud cover reduction along the West coast (and also partly along the Northern boundary of the Sahel) is also an area of mean CTT increase with airborne dust. This may represent suppression of convective activity in this region and may give evidence for an increased stabilisation of the atmospheric layer by dust transported towards the Atlantic Ocean in the Saharan Air Layer (SAL).

The spatial distributions of the net cloud property changes during the Sahelian monsoon season indicate that a cloud cover decrease in the Western and Central parts of the domain is correlated with a CTT increase in the same areas. In the other parts of the domain, mainly cloud cover increases and CTT reductions are observed, also spatially well correlated.

Generally the maps of the spatial distributions of cloud cover and CTT net changes throughout Northern Africa indicate that the shifts in the histograms are not the result of the spatial distributions of dust and clouds, but that these effects are present in a large majority of the grid cells. Moreover they give evidence that the dust-cloud-interactions in the Sahel are not only different by season and air mass, but also that these effects (cloud lifetime effect, atmospheric stabilisation effect) or their respective predominance are distributed spatially over the domain.

Finally it is obvious that for the single grid cells the magnitude of the cloud property change (cloud cover, CTT) often is much higher than the average magnitude throughout the domain (separated by season/air mass). The averaged cloud property change as obtained from the histogram analysis thus is the integral over counteracting effects not only within the observations themselves, but also over the averaging domain. Moreover one could get the impression that the large scale patterns partly point into another direction than the region averaged relationships found from the histogram analysis. One should be aware that the numbers of observations for each grid cell are much lower than for the histogram analysis over the whole region – and thus also the reliability of the statistical results presented in Fig. 8 is lower. Figure 8 should be regarded as a hint only, that the relationships found in the histogram analysis are not the pure result of geographical features of the domain.

The analysis of three different satellite datasets with the same statistical methods gives an estimate of the uncertainty of the results – besides all the orbital and methodological factors discussed above affecting the observations. Generally the SEVIRI dataset is assumed to be the most tightly constrained to certain meteorological conditions (dry air mass, cloud free at day and night), thus the large differences between the SEVIRI results and those of the other satellite datasets mainly reflect the limitations of the BMDI method. On the other hand BMDI is capable of dust detection under conditions where it is not possible with the SYNAER method (over bright desert surfaces). Thus the ENVISAT

dataset can be assumed to be also tightly constrained to a certain subset of the observations. Moreover the overpass time of ENVISAT is not the most favourable for aerosol-cloud-interaction research in the Sahel as discussed. But nevertheless at least the signs of the mean net cloud property changes of all three datasets point into the same direction, which gives some confidence in the results. Moreover although reflecting different limiting conditions, the magnitudes of the cloud cover effect are quite similar between MODIS and ENVISAT whereas those of CTT are more similar between SEVIRI and ENVISAT. The comparison of the detailed results of Table 2 and the mean net changes presented in Table 3 shows that the mean net cloud cover change results from different effects in the different subsets (meteorological conditions) of the total database.

5 Summary

The analysis of five years of daily MODIS Level 3, ENVISAT SYNAER and APOLLO (AATSR) and MSG-SEVIRI BMDI and APOLLO, together with TRMM 3B41 rainfall observations for monsoon season determination, gives a multi-satellite view on relationships between dust aerosol and the cloud state in the West African Sahel.

Often there is no aerosol type discrimination of the observed effects in satellite studies of aerosol-cloud interactions. Here a statistical large-scale analysis of satellite observations of dust-cloud interactions over land is presented. From these observations different relationships between the dust aerosol and cloud cover, cloud top temperature and ice phase fraction are evident.

In the dry season, being characterised by generally low cloud cover in the domain, the suitability of (aged) mineral dust as CCN leads mainly to reduced droplet sizes and to slightly increased convective activity in both flows indicating a contribution of the cloud lifetime effect under low cloudiness (as obtained from the detailed MODIS observations).

During the monsoon season, when most of the regions annual precipitation is produced, the suppression of convective intensity, by an increase of atmospheric stability due to absorbing dust aerosols, and the reduction of cloud droplet sizes, due to the availability of large numbers of CCN, seem to be predominant from this statistical point of view.

As the increase of the atmospheric stability is a direct effect of absorption of solar (and maybe also thermal) radiation, it is directly a function of the absorptivity of the aerosol. Moreover the aerosol type also determines the suitability of the aerosol particles as CCN – or as GCCN. As counteracting effects have been observed here (and also in previous case studies and modelling experiments, e.g. Kaufman and Fraser, 1997 and Perlwitz and Miller, 2010), there is a clear need of aerosol type discrimination in aerosol-cloud-interaction studies.

Although the spatial distribution of the observed net changes generally represents the findings of the seasonally separated histogram analysis (of MODIS observations), it is evident that there are also spatial patterns of these effects within the Sahel, which counteract in the average over the whole domain.

Many studies dealing with indirect aerosol effects concentrate on shortwave radiative forcing and the cloud albedo effect (Twomey, 1974). We did not present cloud albedo or cloud optical depth effects of the aerosol here, because the focus of this study is on impacts of mineral dust load on the cloud state (cover, height, phase). It is clearly evident from the results, especially from the relationships between dust aerosol and cloud cover and cloud top temperature shown here, that not only the amount of reflected shortwave radiation is changed by indirect aerosol effects, but also the outgoing longwave radiation of clouds is subject to aerosol effects on cloud microphysics.

New instruments such as the Infrared Atmospheric Sounder Interferometer (IASI) onboard the MetOp satellite may provide also height information about dust aerosol and clouds. Also active RADAR and LIDAR instruments (e.g. CloudSat, Caliop) provide height information of clouds and aerosol, but so far the database is insufficient due to the much weaker sampling (no across-track scanning). With these new observation methods also the question of interference of aerosol and cloud layers may be addressed in future studies.

References

Albrecht, B. A.: Aerosols, cloud microphysics, and fractional cloudiness, Science, 1227–1230, 1989.

Ackerman, S. A.: Remote sensing aerosols using satellite infrared observations, J. Geophys. Res., 102, 17069–17079, 1997.

Ansmann, A., Tesche, M., Althausen, D., Müller, D., Seifert, P., Freudenthaler, V., Heese, B., Wiegener, M., Pisani, G., Knippertz, P., and Dubovik, O.: Influence of Saharan dust on cloud glaciation in southern Morocco during the Saharan

Mineral Dust Experiment, J. Geophys. Res., 113, D04210, doi:10.1029/2007JD008785, 2008.

Baum, B. A. and Platnick, S.: Introduction to MODIS cloud products, in: Earth Science Satellite Remote Sensing, Vol. 1: Science and instruments, edited by: Qu, J. J., et al., Springer-Verlag, 2006.

Bou Karam, D., Flamant, C., Tulet, P., Todd, M. C., Pelon, J., and Williams, E.: Dry cyclogenesis and dust mobilization in the intertropical discontinuity of the West African Monsoon: A case study, J. Geophys. Res., 114, D05115, doi:10.1029/2008JD010952, 2009.

Brindley, H. and Ignatov, A.: Retrieval of mineral aerosol optical depth and size information from Meteosat Second Generation SEVIRI solar reflectance bands, Remote Sens. Environ., 102, 344–363, 2006.

Carslaw, K. S., Boucher, O., Spracklen, D. V., Mann, G. W., Rae, J. G. L., Woodward, S., and Kulmala, M.: A review of natural aerosol interactions and feedbacks within the Earth system, Atmos. Chem. Phys., 10, 1701–1737, doi:10.5194/acp-10-1701-2010, 2010.

DeMott, P. J., Sassen, K., Poellet, M. R., Baumgardner, D., Rogers, D. C., Brooks, S. D., Prenni, A. J., and Kreidenweis, S. M.: African dust aerosols as atmospheric ice nuclei, Geophys. Res. Lett., 30, 1732, doi:10.1029/2003GL017410, 2003.

Dubovik, O., Holben, B., Eck, T. F., Smirnov, A., Kaufman, Y. J., King, M. D., Tanré, D., and Slutsker, I.: Variability of Absorption and Optical Properties of Key Aerosol Types Observed in Worldwide Locations, J. Atmos. Sci., 59, 590–608, 2002.

Feingold, G., Cotton, W. R., Kreidenweiss, S. M., and Davies, J. T.: The Impact of Giant Cloud Condensation Nuclei on Drizzle Formation in Stratocumulus: Implications for Cloud Radiative Properties, J. Atmos. Sci., 56, 4100–4117, 1999.

Flamant, C., Knippertz, P., Parker, D. J., Chaboureau, J.-P., Lavaysse, C., Agusti-Panareda, A., and Kergoat, L.: The impact of a mesoscale convective system cold pool on the northward propagation of the intertropical discontinuity over West Africa, Q. J. Roy. Meteor. Soc., 135, 139–159, 2009.

Haywood, J. and Boucher, O.: Estimate of the direct and indirect radiative forcing due to tropospheric aerosols: a review, Rev. Geophys., 38, 513–543, 2000.

Holben, B. N., Eck, T. F., Slutsker, I., Tanré, D., Buis, J. P., Setzer, K. A., Vermote, E., Reagan, J. A., Kaufman, Y. J., Nakajima, T., Lavenu, F., Jankowiak, I., and Smirnov, A.: AERONET – A Federated Instrument Network and Data Archive for Aerosol Characterization, Remote Sens. Environ., 66, 1–16, 1998.

Holzer-Popp, T., Schroedter-Homscheidt, M., Breitkreuz, H., Martynenko, D., and Klüser, L.: Improvements of synergetic aerosol retrieval for ENVISAT, Atmos. Chem. Phys., 8, 7651–7672, doi:10.5194/acp-8-7651-2008, 2008.

Hubanks, P. A., King, M. D., Platnick, S. A., and Pincus, R. A.: MODIS Atmosphere L3 Gridded Product Algorithm Theoretical Basis Document, MODIS Algorithm Theoretical Basis Document No. ATBD-MOD-30 for Level-3 Global Gridded Atmosphere Products (08_D3, 08_E3, 08M3), online: http://modis-atmos.gsfc.nasa.gov/_docs/L3_ATBD_2008_12_04.pdf, 2008.

Huffman, G. J., Adler, R. F., Morrissey, M., Bolvin, D. T., Curtis, S., Joyce, R., McGavock, B., and Susskind, J.: Global Precipitation at One-Degree Daily Resolution from Multi-Satellite Observa-tions, J. Hydrometeor., 2(1), 36–50, 2001.

Huffman, G. J., Adler, R. F., Bolvin, D. T., Gu, G., Nelkin, E. J., Bowman, K. P., Hong, Y., Stocker, E. F., and Wolff, D. B.: The TRMM Multi-satellite Precipitation Analysis: Quasi-Global, Multi-Year, Combined-Sensor Precipitation Estimates at Fine Scale, J. Hydrometeor., 8(1), 38–55, 2007.

Hui, W. J., Cook, B. I., Ravi, S., Fuentes, J. D., and D'Odorico, P.: Dust-rainfall feedbacks in the West African Sahel, Water Resources Research, 44, W05202, doi:10.1029/2008WR006885, 2008.

Hsu, N. C., Tsay, S. C., King, M. D., and Herman, J. R.: Aerosol Properties Over Bright-Reflecting Source Regions, IEEE T. Geosci. Remote, 42, 557–569, 2004.

Jenkins, G. S., Pratt, A. S., and Heymsfield, A.: Possible linkages between Saharan dust and tropical cyclone rain band invigoration in the eastern Atlantic during NAMMA-06, Geophys. Res. Lett., 35, L08815, doi:10.1029/2008GL034072, 2008.

Kaufman, Y. J. and Fraser, R. S.: The effect of smoke particles on clouds and climate forcing, Science, 277, 1636–1639, 1997.

Kaufman, Y. J., Tanré, D., and Boucher, O.: A satellite view of aerosols in the climate system, Nature, 419, 215–223, 2002.

King, M. D., Kaufman, Y. J., Tanré, D., and Nakajima, T.: Remote Sensing of Tropospheric Aerosols from Space: Past, Present and Future, B. Am. Meteorol. Soc., 80, 2229–2259, 1999.

King, M. D., Menzel, W. P., Kaufman, Y. J., Tanré, D., Gao, B. C., Platnick, S., Ackerman, S. A., Remer, L. A., Pincus, R., and Hubanks, P. A.: Cloud, Aerosol and Water Vapor Properties from MODIS., IEEE Trans. Geosci. Remote Sens., 41, 442–458, 2003.

Klose, M., Shao, Y., Karremann, M. K., and Fink, A. H.: Sahel dust zone and synoptic background, Geophys. Res. Lett., 37, L09802, doi:10.1029/2010GL042816, 2010.

Klüser, L., Rosenfeld, D., Macke, A., and Holzer-Popp, T.: Observations of shallow convective clouds generated by solar heating of dark smoke plumes, Atmos. Chem. Phys., 8, 2833–2840, doi:10.5194/acp-8-2833-2008, 2008.

Klüser, L. and Schepanski, K.: Remote sensing of mineral dust over land with MSG infrared channels: A new Bitemporal Mineral Dust Index, Remote Sens. Environ., 113, 1853–1867, doi:10.1016/j.rse.2009.04.012, 2009.

Knippertz, P. and Fink, A. H.: Synoptic and dynamic aspects of an extreme springtime Saharan dust outbreak, Q. J. Roy. Meteor. Soc., 132, 1153–1177, 2006.

Kriebel, K. T., Saunders, R. W., and Gesell, G.: Optical properties of clouds derived from fully cloudy AVHRR pixels, Beitr. Phys. Atmosph., 62, 165–171, 1989.

Kriebel, K. T., Gesell, G., Kästner, M., and Mannstein, H.: The cloud analysis tool APOLLO: improvements and validations, Int. J. Rem. Sens., 24, 2389–2408, 2003.

Lebel, A. and Ali, A.: Recent trends in the Central and Western Sahel rainfall regime (1990–2007), J. Hydrol., 375, 52–64, 2009.

Legrand, M., Plana-Fattori, A., and N'doume, C.: Satellite detection of dust using the IR imagery of Meteosat, 1. Infrared Difference Dust Index, J. Geophys. Res., 106, 18251–18274, 2001.

Levy, R. C., Remer, L. A., Kleidman, R. G., Mattoo, S., Ichoku, C., Kahn, R., and Eck, T. F.: Global evaluation of the Collection 5 MODIS dark-target aerosol products over land, Atmos. Chem. Phys. Discuss., 10, 14815–14873, doi:10.5194/acpd-10-14815-2010, 2010.

Li, J., Zhang, P., Schmit, T. J., Schmetz, J., and Menzel, W. P.:

Quantitative monitoring of a Sahara dust event with SEVIRI on Meteosat-8, Int. J. Remote Sens., 28, 2181–2186, 2007.

McConnell, C. L., Highwood, E. J., Coe, H., Formenti, P., Anderson, B., Osborne, S., Nava, S., Desboeufs, K., Chen, G., and Harrision, M. A. J.: Seasonal variations of the physical and optical characteristics of Saharan dust: Results from the Dust Outflow and Deposition to the Ocean (DODO) experiment, J. Geophys. Res., 113, D14S05, doi:10.1029/2007JD009606, 2008.

N'Tchayi Mbourou, G., Bertrand, J. J., and Nicholson, S. E.: The Diurnal and Seasonal Cycles of Wind-Borne Dust over Africa North of the Equator, J. Appl. Meteor., 36, 868–882, 1997.

Parker, D. J., Burton, R. R., Diongue-Niang, A., Ellis, R. J., Felton, M., Taylor, C. M., Thorncroft, C. D., Bessemoulin, P., and Tompkins, A. M.: The diurnal cycle of the West African monsoon circulation, Q. J. Roy. Meteor. Soc., 131, 2839–2860, 2005.

Pavolonis, M. J. and Heidinger, A. K.: Daytime cloud overlap detection from AVHRR and VIIRS, J. Appl. Meteorol., 43, 762–778, 2004.

Perlwitz, J. and Miller, R. L.: Cloud cover increase with increasing absorptivity: A counterexample to the conventional semidirect aerosol effect, J. Geophys. Res., 115, D08203, doi:10.1029/2009JD012637, 2010.

Ramanathan, A., Crutzen, P. J., Kiehl, J. T., and Rosenfeld, D.: Aerosols, climate, and the hydrological cycle, Science, 294, 2119–2124, 2001.

Remer, L. A., Tanré, D., and Kaufman, Y. J.: Algorithm for remote sensing of tropospheric aerosol from MODIS: Collection 005, Algorithm Theor. Basis Doc. ATBD-MOD-02, NASA Goddard Space Flight Cent., Greenbelt, Md. (http://modis.gsfc.nasa.gov/data/atbd/atbd_mod02.pdf), 2006.

Rosenfeld, D., Rudich, Y., and Lahav, R.: Desert dust suppressing precipitation: a possible desertification feedback loop, Proc. Natl. Acad. Sci. USA, 98, 5975–5980, 2001.

Rosenfeld, D.: Aerosol-cloud interactions control of earth radiation and latent heat release budgets, Space Sci. Rev., 125, 149–157, 2006.

Rudich, Y., Khersonsky, O., and Rosenfeld, D.: Treating clouds with a grain of salt, Geophys. Res. Lett., 29(22), 2060, doi:10.1029/2002GL016055, 2002.

Saunders, R. W. and Kriebel, K. T.: An improved method for detecting clear sky and cloudy radiances from AVHRR data, Int. J. Remote Sens., 9, 123–150, 1988.

Stevens, B. and Feingold, G.: Untangling aerosol effects on clouds and precipitation in a buffered system, Nature, 461, 607–613, doi:10.1038/nature08281, 2009.

Tulet, P., Mallet, M., Pont, V., Pelon, J., and Boone, A.: The 7–13 March 2006 dust storm over West Africa: Generation, transport, and vertical stratification, J. Geophys. Res., 113, D00C08, doi:10.1029/2008JD009871, 2008.

Twomey, S.: Pollution and the planetary albedo, Atmos. Environ., 8, 1251–1256, 1974.